World Academy of Science, Engineering and Technology
International Journal of Mechanical and Mechatronics Engineering
Vol:11, No:6, 2017

Assessment of Modern RANS Models for the C3X Vane Film Cooling Prediction

Mikhail Gritskevich, Sebastian Hohenstein

***Abstract*—**The paper presents the results of a detailed assessment of several modern Reynolds Averaged Navier-Stokes (RANS) turbulence models for prediction of C3X vane film cooling at various injection regimes. Three models are considered, namely the Shear Stress Transport (SST) model, the modification of the SST model accounting for the streamlines curvature (SST-CC), and the Explicit Algebraic Reynolds Stress Model (EARSM). It is shown that all the considered models face with a problem in prediction of the adiabatic effectiveness in the vicinity of the cooling holes; however, accounting for the Reynolds stress anisotropy within the EARSM model noticeably increases the solution accuracy. On the other hand, further downstream all the models provide a reasonable agreement with the experimental data for the adiabatic effectiveness and among the considered models the most accurate results are obtained with the use EARMS.

***Keywords*—**Discrete holes film cooling, Reynolds Averaged Navier-Stokes, Reynolds stress tensor anisotropy, turbulent heat transfer.

I. Introduction

NOWADAYS, the efficiency of modern industrial gas turbines strongly relies on the elevation of the gas-path temperature, which makes the turbine blades subjected to extremely high thermal loads. The common way of protecting the blade is to introduce a kind of film cooling for which the coolant is injected from discrete holes forming a relatively cold film along the blade surface.

One of the known problems of the film cooling is its reduced effectiveness in case of high blowing ratios [1], for which the coolant jets penetrate deep into the gas-path resulting in limited film coverage downstream of the holes. At the same time, due to the jet-mainstream interaction the additional aerodynamic losses are introduced, which potentially reduce or even eliminate the efficiency gain due the gas temperature elevation. Therefore, a detailed understanding of the heat transfer mechanisms is essential for improvement of cooling systems. For that purpose, the Computational Fluid Dynamics (CFD) methods are widely employed providing three-dimensional velocity and temperature fields, which could be used for the design of elaborated film cooling configurations. It should be however noted, however, that the precise prediction of the lateral spread and vertical penetration of a film cooling jet is far from being straightforward since it requires an accurate specification of the Reynolds stress tensor anisotropy [2], [3]. For that purpose, the most suitable approach is to apply Scaled Resolving Simulations (SRS) [4], [5] (e.g. Detached Eddy Simulation, Large Eddy Simulation or even Direct Numerical Simulation), which have been successfully applied for prediction of the film cooling for both flat plates [6]-[11] and airfoils [12]-[16]. However, despite the significant progress reached in the development and application of SRS approaches they still remain prohibitively expensive when complex geometries with multiple turbulent scales are considered. Moreover, if more than one row of blades has to be modeled in the framework of SRS the simulation without any circumferential periodicity should be performed to be able to properly specify the conditions at the rotor/stator interfaces [17], which is far beyond the capabilities of modern computers. Therefore, taking into account the relatively high computation cost of SRS approaches the engineering simulations of the film cooling are conventionally performed with the use of the RANS equations [2], [3]. It should be noted, however, that due to the turbulence closure problem RANS strongly relies on the baseline turbulence model [18] and often tend to incorrectly predict the flows with a separation or strong anisotropy of the Reynolds stress tensor (unless it is somehow accounted within the model), which is the case for a typical film cooling configuration. Particularly, it is widely acknowledged that the RANS models with a linear relation between the Reynolds stress and strain rate tensors are incapable to predict the peculiarities of the jet-mainstream interaction in the vicinity of the holes [2], [3], while further downstream they could provide a reasonable agreement with the experimental data [19]-[27]. On the other hand, as of today the information about the performance of the RANS models accounting for the Reynolds stress anisotropy is somehow contradictory [2], [3], which makes a detailed assessment of their accuracy and robustness, when applied to the film cooling prediction, of a high practical importance. For that purpose, three models are considered within the current paper, namely the SST model [28], the modification of the SST model accounting for the streamlines curvature (SST-CC) [29], and the EARSM [30], which accounts for the Reynolds stress anisotropy by introducing the additional non-linear terms based on the strain rate tensor invariants. It should be noted that these models utilize similar equations for the turbulence kinetic energy and for the specific dissipation rate, which allows distinguishing the effects due to the Reynolds stress anisotropy with those due to the baseline model performance.

The accuracy and robustness of the abovementioned

M. Gritskevich is with Siemens LLC, St. Petersburg, Volynskiy Lane 3A, 191186, Russia (phone: +7-812-329-8598; e-mail: mikhail.gritckevich@siemens.com).

S. Hohenstein is with Siemens AG, Muelheim an der Ruhr, Mellinghofer Str. 55, 45473, Germany (e-mail: sebastian.hohenstein@siemens.com).

turbulence models are assessed for the flow around the C3X vane with and without film cooling [31], [32] under the flow conditions typical for the first stage turbine vanes. For all the simulations, the governing equations are solved in the steady state formulation for the ideal compressible gas with the use of the ANSYS-CFX general purpose CFD code.

II. Description of Flow around the C3X Vane

The C3X vane cascade has been experimentally studied in [31], [32]. The geometry of each vane corresponds to a scaled two-dimensional slice from a first-stage nozzle for a helicopter engine. The experiment is conducted at the inlet Mach number Ma_{in}=0.08 and at the inlet Reynolds number Re_{in}=2.3·10^5 based on the vane chord C. These conditions are comparable to a first vane of a small helicopter gas turbine engine at a sea level takeoff. For the film cooling one linear and two staggered rows of holes with the diameter D are considered with the holes inclined in the streamwise direction at the angle of 30° and distributed in the spanwise direction with the spacing of 3D.

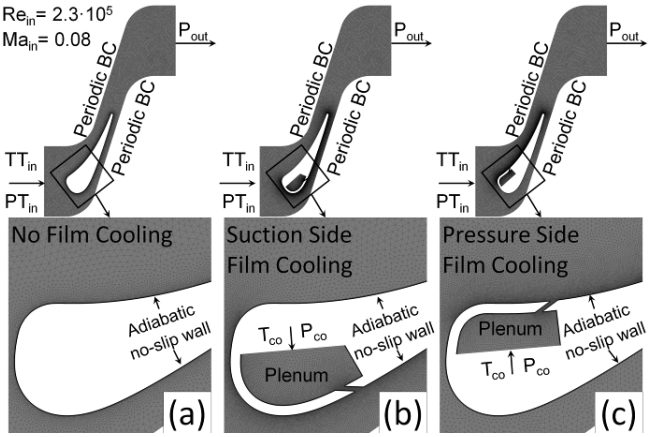

Fig. 1 Computational setup for the C3X vane: (a) No cooling; (b) Suction side cooling; (c) Pressure side cooling

The computational domains and the computational grids for the considered configurations of the C3X vane are shown in Fig. 1. The inlet section corresponds to the location of the experimental measurements of the velocity and turbulence quantities, which allows the precise specification of the boundary conditions.

The computational grid consists of 0.7-4.5 million cells depending on the configuration (the preliminary study justifies that the considered grids provide the grid independent solutions) and has a dense clustering towards the vane surface and the plenum walls to ensure Δy^+<1 in the entire domain.

At the inlet, the total temperature (TT_{in}) and total pressure (PT_{in}) as well as the turbulence quantities are specified (Fig. 1), which correspond to relatively high-level large-scale turbulence closely representative of turbulence conditions being believed to be typical at the inlet to first stage vanes. At the outlet boundary, the static pressure (P_{out}) is set, whereas the remaining transported quantities are extrapolated from the domain. On the vane surface a no-slip adiabatic condition is employed. A symmetry condition is applied in the spanwise direction, and a periodic condition is utilized at the top and bottom boundaries.

Finally, at the plenum inlet the constant pressure (P_{CO}) and temperature (T_{CO}) are set, whereas a no-slip adiabatic condition is employed at the solid walls. Unlike the T_{CO} values, which are known from the experiment, the P_{CO} values are iteratively adjusted to fit the experimental velocity ratio (VR) at the outlet from the holes (the constant density ratio of DR=0.94 is used for all the considered injection regimes).

III. Assessment of the Considered Turbulence Models for the C3X Vane Test Case

In this section the considered turbulence models are assessed for the prediction of the flow around the C3X vane with and without film cooling. The experimental data comprise the measurements of the wall pressure and temperature for the case without film cooling as well as the adiabatic effectiveness for both the pressure and suction side film cooling from either one or two rows of holes.

A. No Film Cooling

The obtained distributions along the C3X vane without film cooling are shown in Fig. 2.

As seen, all the considered models yield almost identical pressure distributions which are in a relatively good agreement with the experimental data. Similarly, all the considered models yield close distributions of the skin friction coefficient; however, at the suctions side the maximum of the skin friction coefficient slightly depends on the peculiarities of the Reynolds stress modeling due to the strong curvature of the vane accompanied with the flow acceleration.

With regards to the vane temperature, almost perfect agreement with the experimental data is observed in the vicinity of the stagnation point for all the considered models.

Consistently with the skin friction coefficient, all the considered models yield almost identical temperature distributions at the pressure side, which are in a reasonable agreement with the experimental data; however, the level of the wall temperature is slightly overestimated for x/C>0.2, whereas the slope and the shape of the calculated curves are similar to the experimental distribution. It should be mentioned that the experimental temperature distributions have a non-monotonic behavior at x/C≈0.2, which origin is not clear from the description of the experiment [31], [32].

Finally, the difference between the models at the suction side is noticeably larger than those at the pressure side. Particularly, SST and SST-CC yield close to the experimental results; however, the minimum value at x/C≈0.35 is slightly overestimated. At the same time, EARSM slightly delays the temperature recovery (however, the slope of the curve is similar to those of the experiment) and slightly underestimates the temperature minimum.

B. Suction Side Film Cooling

To illustrate the topology of the flow and to outline the peculiarities of the suction side film cooling the contours of

the adiabatic effectiveness and iso-surfaces of the λ_2 criterion obtained with the use of SST are shown in Fig. 3 (for the other two models, similar topology is obtained). As seen, the pronounced counter-rotating vortex pair and the horseshoe vortex typical for the jet in the cross-flow are observed for all the considered injection regimes.

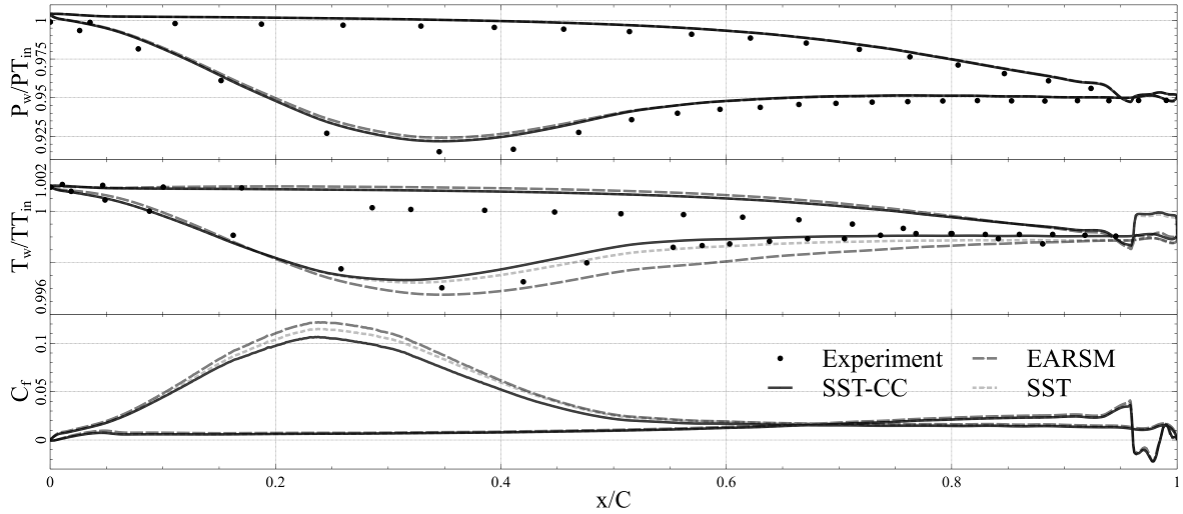

Fig. 2 Distributions of the wall pressure, wall temperature, and skin friction coefficient along the C3X vane

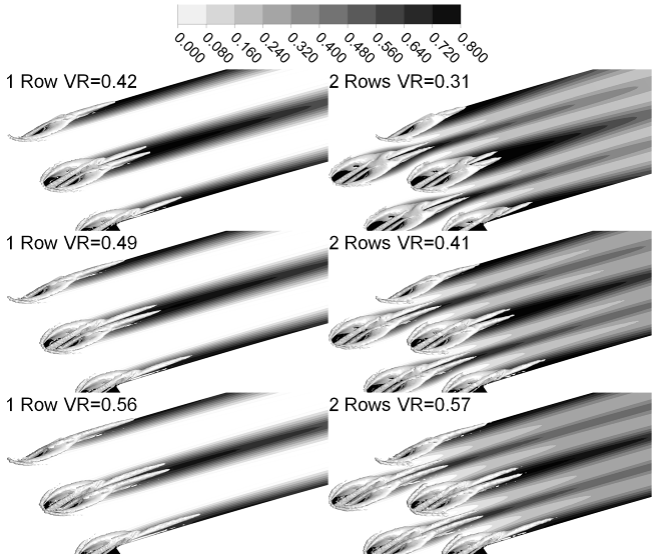

Fig. 3 Contours of the adiabatic effectiveness and iso-surfaces of the λ_2 criterion at the suction side for the SST model

With regards to the adiabatic effectiveness contours, due to the relatively low velocity ratios the jet emanating from the holes is forced to the vane surface resulting in an amplification of the film cooling effectiveness downstream. As expected, due to the denser arrangement, the configuration with two staggered rows yields better lateral film coverage of the vane surface than those of one row; however, for all the considered injection regimes the distinct traces of both upstream and downstream jets could be observed indicating that the interaction between the successive jets is marginal.

To make a quantitative comparison between the considered turbulence models, the skin friction coefficient profiles are shown in Fig. 4. As seen, accounting for the streamlines curvature of the SST-CC model has marginal effect on the solution and the obtained profiles are very close to those of SST, whereas accounting for the Reynolds stress anisotropy within EARSM has a noticeably larger effect on the solution. Particularly, for all the considered injection regimes SST and SST-CC yield fully attached flow in the vicinity of holes with strongly non-uniform profiles due to the jet-mainstream interaction, whereas EARSM predicts a small separation zone for two staggered rows at VR=0.31. Further downstream, as the jets are penetrating into the mainstream, the uniform profiles are recovering; however, the recovery rate of EARMS is noticeably slower than those of the other two models.

With regards to the spanwise distributions of the adiabatic effectiveness (Fig. 5), the most noticeable difference between SST and SST-CC is observed in the vicinity of the holes. Particularly, SST-CC yields slightly lower maximum of the adiabatic effectiveness at x/D=1.0 than those of SST, whereas further downstream the difference between the models is diminishing indicating that the effect of the curvature correction is marginal in that region. With regards to EARMS, it yields slightly higher adiabatic effectiveness in the vicinity of the holes (x/D=1.0), and at the same time, more rapid decay of the maximum adiabatic effectiveness further downstream for all the considered injection regimes (it should be noted that the shape of the EARSM profile is also noticeably different from those of SST and SST-CC).

Finally, to compare the obtained results with the experiment, the axial distributions of the adiabatic effectiveness at the mid-span section (z/D=0.75) is depicted in Figs. 6 and 7. As seen, all the considered models noticeably underestimate the adiabatic effectiveness in the vicinity of the holes, which is likely explained by inaccurate prediction of the lateral heat diffusion typical for the models utilizing a linear relation between the eddy viscosity and turbulent heat flux

[33]. Further downstream, as the jets are penetrating deeper into the mainstream, all the considered models predict similar distributions (however, SST and SST-CC yield slightly higher adiabatic efficiency comparing to those of EARSM), which are in a good agreement with the experimental data for all the considered injection regimes.

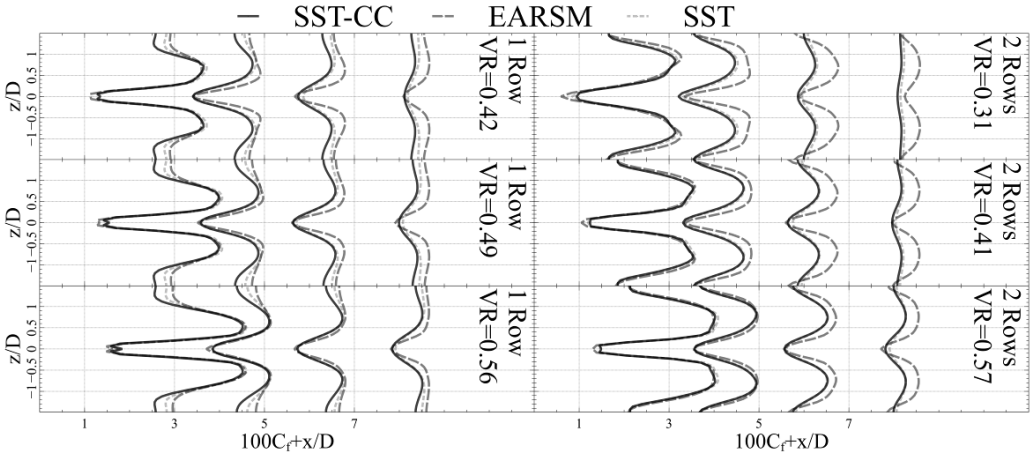

Fig. 4 Spanwise distributions of the skin friction coefficient at the suction side at different axial sections (*x/D*=1, 3, 5, 7)

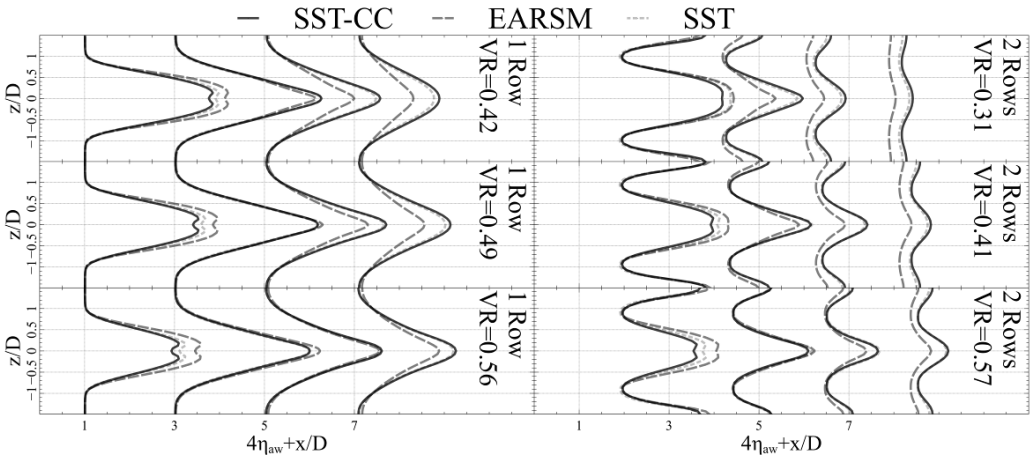

Fig. 5 Spanwise distributions of the adiabatic effectiveness at the suction side at different axial sections (*x/D*=1, 3, 5, 7)

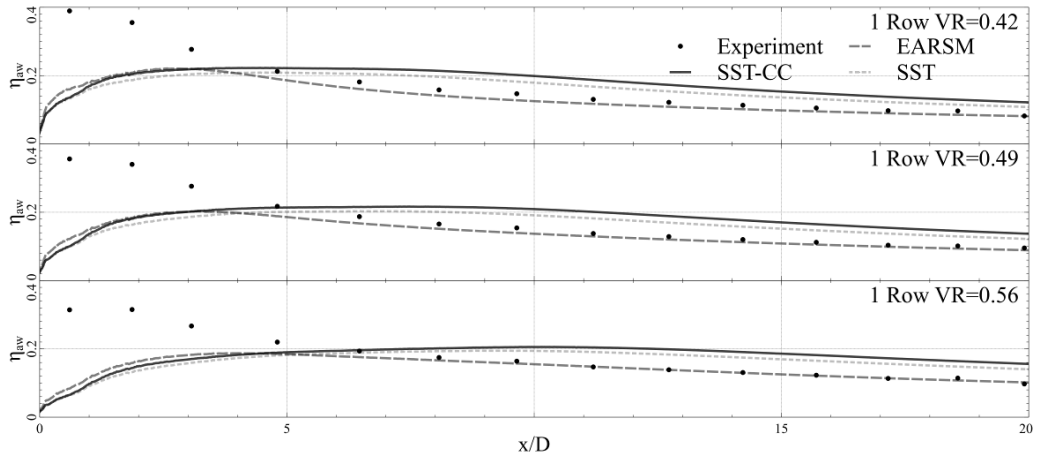

Fig. 6 Axial distribution of the adiabatic effectiveness at the mid-span section (*z/D*=0.75) for one row of holes at the suction side.

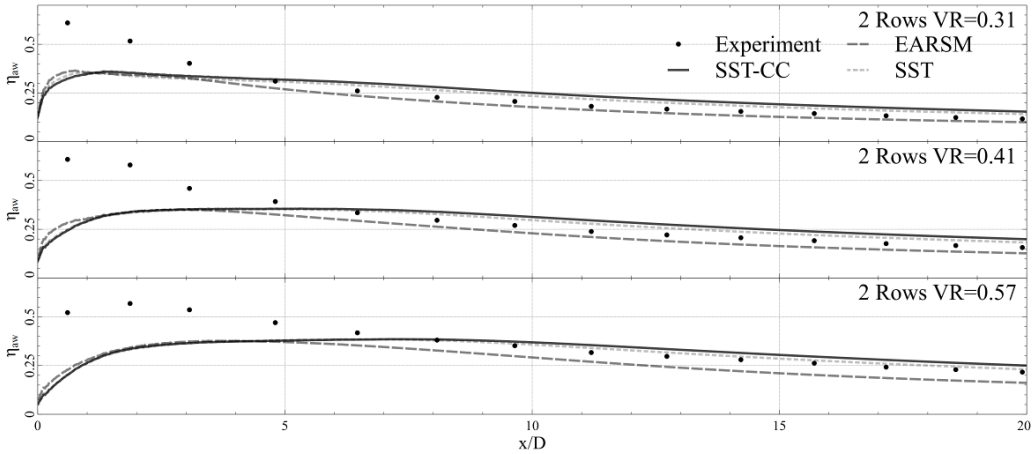

Fig. 7 Axial distribution of the adiabatic effectiveness at the mid-span section (z/D=0.75) for two rows of holes at the suction side

C. Pressure Side Film Cooling

Similar to the suction side film cooling, the topology of the flow is illustrated with the use of the adiabatic effectiveness contours and iso-surfaces of the λ_2 criterion for SST at different injection regimes (Fig. 8). As seen, the intensity of the vortex pair is substantially amplifying with the increase of the VR (recall that the range of VR at the pressure side is noticeably larger than those at the suction side), which likely results in more intensive interaction between the jets in case of two staggered rows.

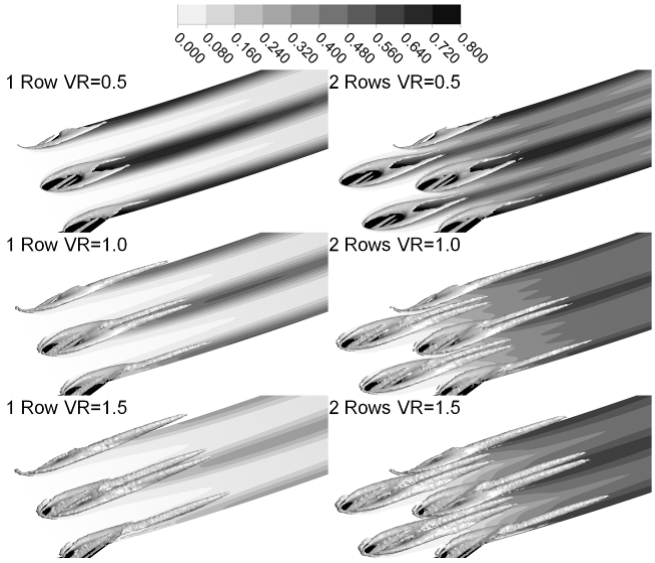

Fig. 8 Contours of the adiabatic effectiveness and iso-surfaces of the λ_2 criterion at the pressure side for the SST model

With regards to the adiabatic effectiveness the contours for one row are close to those at the suction side (however, at the suction side noticeably less effective cooling between two successive holes is observed). At the same time, for two staggered rows the contours of the adiabatic effectiveness for VR=0.5 are similar to those at the suction side, whereas for VR=1.0 and VR=1.5 the coolant emanating from the upstream row is likely isolated from the vane surface since no pronounced traces of the relatively high adiabatic effectiveness are recognized (for the downstream row the traces are similar to those at the suction side).

The peculiarities of the flow prediction with the use of the considered turbulence model are shown in Fig. 9, where the skin friction distributions at different axial sections are illustrated. As seen, unlike the suction side, for which almost fully attached flow has been observed, all the considered models predict a pronounced separation zone in the vicinity of the downstream row of holes in which size is increasing with the increase of VR. It should be noted that the difference between the considered models is noticeably smaller comparing to those at the suction side indicating that the flow is less sensitive to the Reynolds stress anisotropy modeling approach.

To illustrate the peculiarities of the heat transfer due to the interaction between the jets and the vane surface the spanwise distributions of the adiabatic effectiveness at different axial positions are shown in Fig. 10. As seen, the distributions for VR=0.5 are similar to those at the suction side for all the considered models. Particularly, SST and SST-CC yield almost identical results with a slower recovery of the adiabatic effectiveness downstream of the holes comparing to those of EARSM. In contrast, for VR=1.0 and VR=1.5 the spanwise variation of the adiabatic effectiveness in the vicinity of the holes are noticeably smaller comparing to VR=0.5 (it should be noted that similarly to VR=0.5 SST and SST-CC provide identical solutions with the slightly smaller maximum of the adiabatic effectiveness than those of EARSM). Moreover, for all the considered models two pronounced peaks of the adiabatic effectiveness are observed in the vicinity of the downstream row at x/D=1.0, which is likely due to the presence of the recirculation zone in this region. Further downstream the jets are forced to the wall resulting in increase of the adiabatic effectiveness for both one and two rows of holes.

Finally, the mid-span (z/D=0.75) distributions of the adiabatic effectiveness are compared to the experimental data in Figs. 11 and 12.

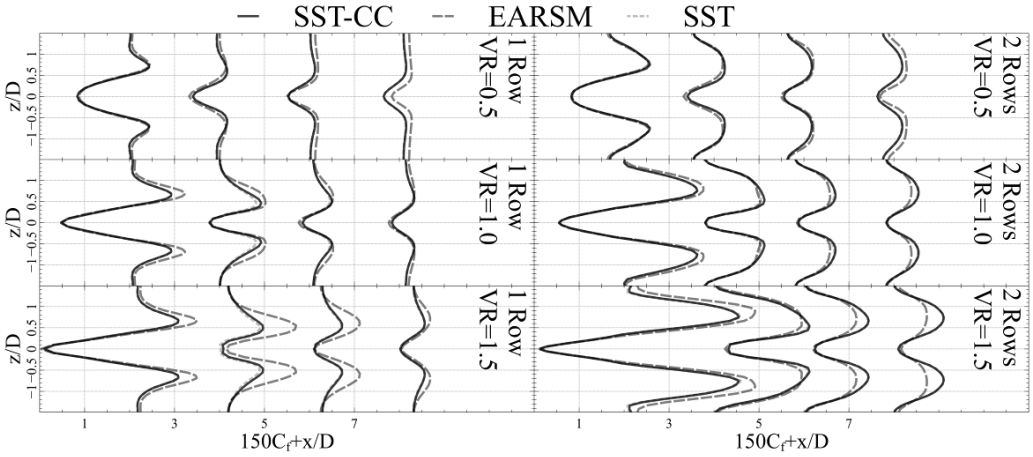

Fig. 9 Spanwise distribution of the skin friction coefficient at the pressure side at different axial sections (*x/D*=1, 3, 5, 7)

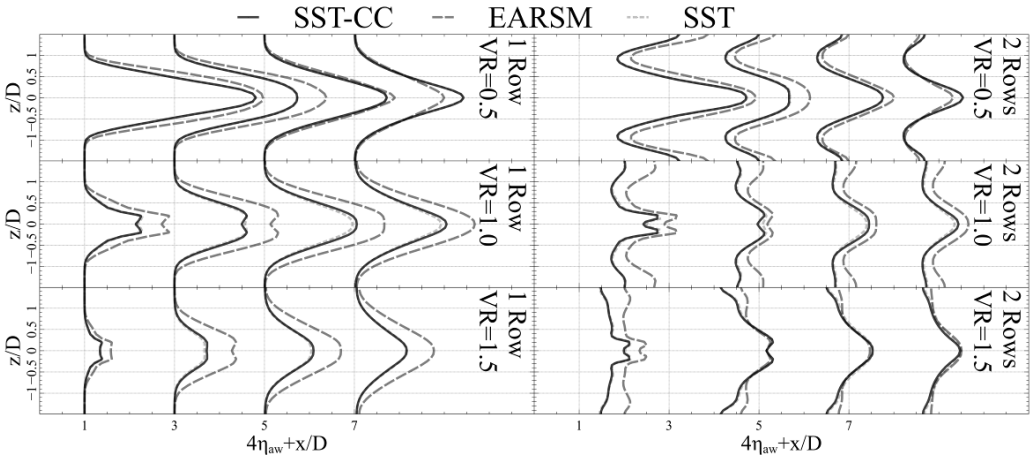

Fig. 10 Spanwise distribution of the adiabatic effectiveness at the pressure side at different axial sections (*x/D*=1, 3, 5, 7)

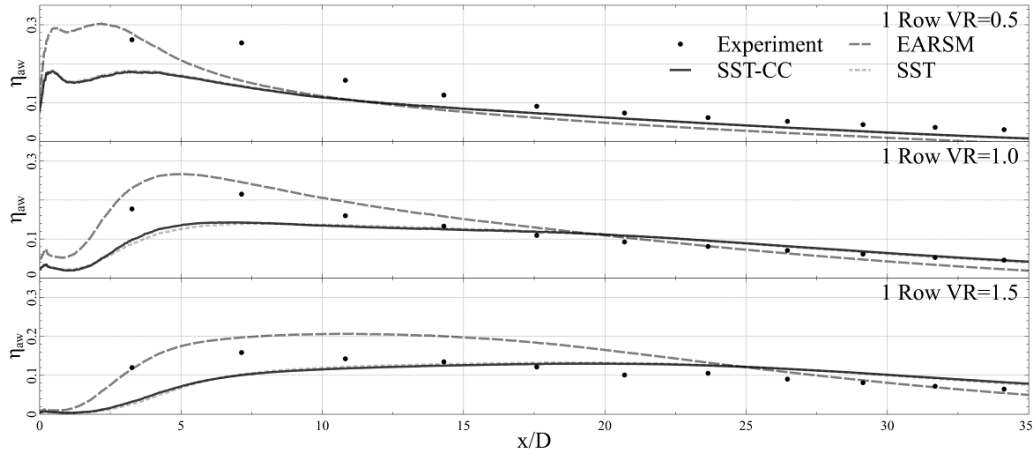

Fig. 11 Axial distribution of the adiabatic effectiveness at the mid-span section (*z/D*=0.75) for one row of holes at the pressure side

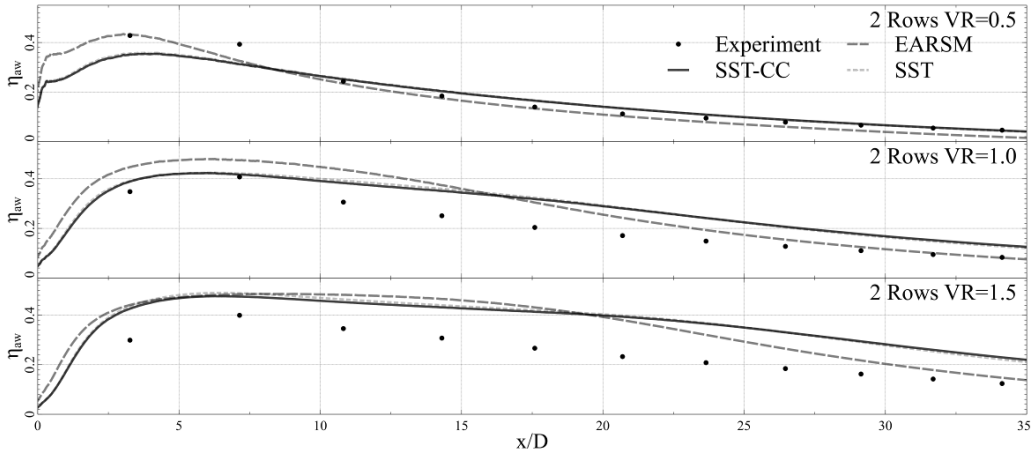

Fig. 12 Axial distribution of the adiabatic effectiveness at the mid-span section (z/D=0.75) for two rows of holes at the pressure side

As expected, the most noticeable difference between the models is observed for one row in the vicinity of holes, where due to the accounting for the Reynolds stress anisotropy EARSM yields noticeably better (however, not perfect) agreement with the experimental data comparing to SST and SST-CC (again the curvature correction has negligible effect on the adiabatic effectiveness).

Similar conclusions could be drawn based on the results for two staggered rows of holes (Fig. 12). Particularly, for all the considered injection regimes EARMS yields better agreement with the experiment than SST and SST-CC (consistently with the previous observation the effect of the curvature correction is marginal); however, the difference between the considered models is less pronounced than for the case of one row of holes.

IV. Conclusion

An assessment of several turbulence models has been performed for the C3X vane with and without film cooling.

The obtained results show that all the considered models yield a relatively good agreement with the experimental data for the case without film cooling. At the same time, it has been shown that accounting for the streamlines curvature within SST-CC and for the Reynolds stress anisotropy within EARSM has only marginal effect on the distributions along the vane surface.

With regards to the cases with film cooling, for all the considered injection regimes, the models have difficulties in prediction of the heat transfer in the vicinity of the holes, especially for the high velocity ratios, whereas further downstream the results are in a relatively good agreement with the experimental data not only for a single row of holes but also for two staggered rows.

Finally, the streamlines curvature correction of SST-CC has a marginal effect on the solution, whereas accounting for the Reynolds stress anisotropy within EARSM noticeably improves the agreement with the experiment but still is not a complete remedy in the vicinity of the holes, where more elaborated turbulence modeling approaches should be considered (e.g. accounting not only for the Reynolds stress anisotropy but also for the turbulent heat flux anisotropy). It should be noted, however, that from a practical point of view the peculiarities of the heat transfer in the vicinity of holes are not of a high importance once the flow downstream is correctly predicted, and thus, EARSM model could be recommended for the engineering simulations.

References

[1] Bunker R.S., "A review of shaped hole turbine film-cooling technology," Journal of Heat Transfer, vol. 127(4), 2005, pp. 441-453.
[2] Mahesh K., "The interaction of jets with crossflow," Annual Review of Fluid Mechanics, vol. 45, pp. 379-407.
[3] Acharya S., Tyagi M., and Hoda A., "Flow and heat transfer predictions for film cooling," Annals of the New York Academy of Sciences, vol. 934(1), 2001, pp. 110-125.
[4] Menter F.R., Schutze J., Kurbatskii K.A., Gritskevich M.S., and Garbaruk A.V., "Scale-resolving simulation techniques in industrial CFD," AIAA Paper 2011–3474, 2011, pp. 708–720.
[5] Menter F.R., Schütze J., and Gritskevich M.S., "Global vs. zonal approaches in hybrid RANS-LES turbulence modeling," Progress in Hybrid RANS-LES Modelling, vol. 117, 2012, pp. 15–28.
[6] Leedom D. H., Acharya S., "Large eddy simulations of film cooling flow fields from cylindrical and shaped holes," Proceedings of ASME Turbo Expo 2008, 2008, pp. 865-877.
[7] Tyagi M., Acharya S., "Large eddy simulation of film cooling flow from an inclined cylindrical jet," Journal of Turbomachinery, vol. 125(4), 2003, pp. 734-742.
[8] Guo X., Schroder W., and Meinke M., "Large eddy simulations of film cooling flows," Computers and Fluids, vol. 35, 2006, pp. 587-606.
[9] Peet Y.V., Lele S.K., "Near field of film cooling jet issued into a flat plate boundary layer: LES study," Proceedings of ASME Turbo Expo 2008, 2008, pp. 409-418.
[10] Renze, P., Schröder W., and Meinke M., "Large-eddy simulation of film cooling flows with variable density jets," Flow Turbulence and Combustion, vol. 80, 2008, pp. 119–132.
[11] Rozati A., Tafti D.K., "Large eddy simulation of leading edge film cooling—part II: heat transfer and effect of blowing ratio," Journal of Turbomachinery, vol. 130(4), 2008, p. 041015.
[12] Rozati A., Tafti D.K., "Effect of coolant-mainstream blowing ratio on leading edge film cooling flow and heat transfer," International Journal of Heat and Fluid Flow, vol. 29(4), 2008, pp. 857–873.
[13] Rozati A., Tafti D.K., "Large-eddy simulations of leading edge film cooling: analysis of flow structures, effectiveness, and heat transfer coefficient," International Journal of Heat and Fluid Flow, vol. 29(1), 2008, pp. 1–17.
[14] Joo J., Durbin P. "Simulation of turbine blade trailing edge cooling" Journal of Fluids Engineering, vol. 131, 2009, pp. 021102.
[15] Liang J., Kang S., "Investigation of film cooling on the leading edge of turbine blade based on detached eddy simulation," Science China Technological Sciences, vol. 55(8), 2012, pp. 2191–2198.

[16] Ravelli S., Barigozzi G., "Modelling the influence of vortex shedding on trailing edge cutback film cooling at different blowing ratios," Proceedings of 11th European Conference on Turbomachinery Fluid dynamics & Thermodynamics, 2015, pp. 1-11.
[17] He L., "Fourier methods for turbomachinery applications," Progress in Aerospace Sciences, vol. 46, 2010, pp. 329–341.
[18] Wilcox D.C., *Turbulence modeling for CFD*, 2006, pp. 1-536
[19] Hasanpour A., Farhadi M., and Ashorynejad H.R., "Hole configuration effect on turbine blade cooling," International Journal of Mechanical, Aerospace, Industrial, Mechatronic and Manufacturing Engineering, vol. 5(1), 2011, pp 1089-1093.
[20] Medic, G., Durbin P.A., "Toward improved film cooling prediction," Journal of Turbomachinery, vol. 124(2), 2002, pp. 193-199.
[21] Johnson J.J. et al.,"Three-dimensional film-cooled vane CFD simulations and preliminary comparison to experiments," AIAA Paper 2011-499, 2011, pp. 1-13.
[22] Bradley A. et al., "Towards efficient CFD-simulations of engine like turbine guide vane film cooling," AIAA Paper, 2011-708, 2011, pp. 1-8.
[23] Najafabadi H.N et al., "CFD simulations using reduced models for film cooling design," AIAA Paper 2011-710, pp. 1-12.
[24] Nasir S. et al., "Effects of large scale high freestream turbulence and exit Reynolds number on turbine vane heat transfer in a transonic cascade," Journal of Turbomachinery, vol. 131(2), 2009, pp. 021021.
[25] Garg, V.K., Ameri, A.A., "Comparison of two-equation turbulence models for prediction of heat transfer on film-cooled turbine blades," Numerical Heat Transfer, vol. 32, 1997, pp. 347-371.
[26] Laskowski G.M., Tolpadi A.K., and Ostrowski M.C., "Heat transfer predictions of film cooled stationary turbine airfoils," Proceedings of ASME Turbo Expo 2007, 2007, pp. 475-485.
[27] Najafabadi H.N., Karlsson M., Utriainen E., and Kinell M., "CFD based sensitivity analysis of influencing flow parameters for cylindrical and shaped holes in a gas turbine vane," Proceedings of ASME Turbo Expo 2012, 2012, pp. 1501-1509.
[28] Menter F.R., Kuntz M., and Langtry R., "Ten years of industrial experience with the SST turbulence model," Turbulence, Heat and Mass Transfer 4, 2003, pp. 625-632.
[29] Smirnov P.E., Menter F.R., "Sensitization of the SST Turbulence model to rotation and curvature by applying the Spalart–Shur correction term," Journal of Turbomachinery, vol. 131(4), 2009, pp. 41010.
[30] Menter F.R., Garbaruk A.V., and Egorov. Y., "Explicit algebraic Reynolds stress models for anisotropic wall-bounded flows," Progress in Flight Physics 3, 2012, pp. 89-104.
[31] Ames F.E., "Aspects of vane film cooling with high turbulence: part I—heat transfer," Journal of Turbomachinery, vol. 120(4), 1998, pp. 768-776.
[32] Ames F.E., "Aspects of vane film cooling with high turbulence: part II—adiabatic effectiveness," Journal of Turbomachinery, vol. 120(4), 1998, pp. 777-784.
[33] Azzi A., Lakehal D., "Perspectives in modeling film cooling of turbine blades by transcending conventional two-equation turbulence models," Journal of Turbomachinery, vol. 124(3), 2002, pp. 472-484.